Influence of Nanohelical Shape and Periodicity on Stem Cell Fate

Rajat K. Das,[†,§] Omar F. Zouani,[†,§,*] Christine Labrugère,[‡] Reiko Oda,[†] and Marie-Christine Durrieu[†]

[†]UMR 5248 CBMN, CNRS—Université de Bordeaux—ENITAB, Institut Européen de Chimie et Biologie, 2 Rue Robert Escarpit, F-33607 Pessac, France and [‡]Université de Bordeaux—CNRS, ICMCB, 87 Avenue du Dr Albert Schweitzer, 33608, Pessac, France. [§]R.K.D. and O.F.Z. contributed equally to this work.

ABSTRACT Microenvironments such as protein composition, physical features, geometry, and elasticity play important roles in stem cell lineage specification. The components of the extracellular matrix are known to subsequently assemble into fibrillar networks *in vivo* with defined periodicity. However, the effect of the most critical parameter, which involves the periodicity of these fibrillar networks, on the stem cell fate is not yet investigated. Here, we show the effect of synthetic fibrillar networks patterned with nanometric periodicities, using bottom-up approaches, on the response of stem cells. We have used helical organic nanoribbons based on self-assemblies of Gemini-type amphiphiles to access chiral silica nanoribbons with two different shapes and periodicities (twisted ribbons and helical ribbons) from the same native self-assembled organic nanostructure. We demonstrate the covalent grafting of these silica nanoribbons onto activated glass substrates and the influence of this programmed isotropically oriented matrix to direct the commitment of human mesenchymal stem cells (hMSCs) into osteoblast lineage *in vitro*, free of osteogenic-inducing media. The specific periodicity of 63 nm (±5 nm) with helical ribbon shape induces specific cell adhesion through the fibrillar focal adhesion formation and leads to stem cell commitment into osteoblast lineage. In contrast, the matrix of periodicity 100 nm (±15 nm) with twisted ribbon shape does not lead to osteoblast commitment. The inhibition of non-muscle myosin II with blebbistatin is sufficient to block this osteoblast commitment on helical nanoribbon matrix, demonstrating that stem cells interpret the nanohelical shape and periodicity environment physically. These results indicate that hMSCs could interpret nanohelical shape and periodicity in the same way they sense microenvironment elasticity. This provides a promising tool to promote hMSC osteogenic capacity, which can be exploited in a 3D scaffold for bone tissue engineering.

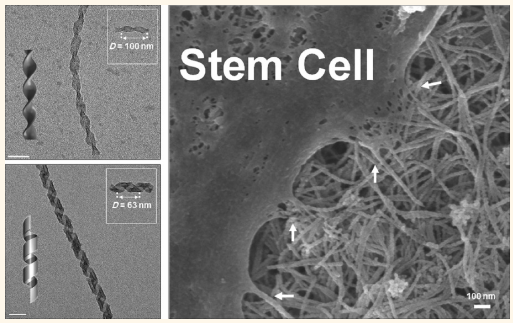

KEYWORDS: silica nanostructures · nanohelical periodicity · surface functionalization · stem cell microenvironment · cell differentiation

Research on the construction of synthetic mimics of extracellular matrix (ECM) has profound implications in the field of regenerative medicine and tissue engineering.[1,2] The complexity of the ECM structure and the intricate interactions of this microenvironment with the adult stem cells, which subtly direct many of the cellular processes, have been intensively investigated.[3−6] In recent years, organic−inorganic biocomposite materials are being increasingly explored as the scaffold to support cell proliferation and differentiation,[7] crucial for the healing of damaged tissues. Meanwhile, self-assembled biocompatible organic nanofibers have been exploited as matrix to (1) present biological epitopes on the fiber surface to establish specific signaling to the cells to promote processes such as angiogenesis and vascularization,[8] but also to (2) assist biomineralization helping the matrix to efficiently integrate into the damaged tissue area and completing the regeneration of tissues.[9] It has clearly been established that nano- and microscale topographical features of ECM mimetic substrates dramatically influence the cell behavior.[5,10−15]

In vivo, ECM is first secreted by cells and subsequently assembled into fibrillar networks that provide crucial mechanical properties to organisms.[16] Biochemical activity by peptide sequences such as RGD (Arg-Gly-Asp) is present in a variety of adhesive proteins forming these fibrillar networks.[16] Recent works indicated that, beyond the chemical specificity of the adhesive epitope, many physical features of the adhesive surface, including its geometry, rigidity, and precise epitope spacing, are critical for guiding receptor-mediated adhesion formation and signaling.[17] However, the effect of the most

* Address correspondence to omar.zouani@inserm.fr.

Received for review January 9, 2013 and accepted March 2, 2013.

Published online March 03, 2013
10.1021/nn4001325

critical parameter, which involves the periodicity of these fibrillar networks, on stem cell fate is not yet investigated. For example, collagen fibrils consisting of high-aspect-ratio polypeptides, the dominating material in the ECM controlling its stiffness, have a periodicity known as the D-band, where D = 67 nm.[18] This periodicity seems to play an important role in the induction of several diseases.[19,20] Indeed, more than 70 mutations in the structural genes for type I procollagen have been found in probands with osteogenesis imperfecta, a heritable disease of children characterized by fragility of bone and other tissues rich in type I collagen.[16,20−23] The mutations include deletions, insertions, RNA splicing mutations, and single-base substitutions that convert a codon for glycine to a codon for an amino acid with a bulkier side chain. At the structural level, these gene mutations are reflected by a change in the periodicity[24] and altered stress distribution on the fibrils, affecting the hierarchical organization of these fibrils, resulting eventually in shape distortion and reduced mechanical strength of the mineralized matrix.[25] It seems therefore to be of prime importance to investigate the role of the structural aspect of these ECMs, in particular the effects the periodicity of these fibrillar structures on the cell fate.

In the past decade, we have developed nonchiral cationic bis-quaternary ammonium gemini surfactants [C_2H_4-1,2-($(CH_3)_2N^+C_nH_{2n+1})_2$], denoted as $n-2-n$, which self-assemble into high-aspect-ratio chiral nanostructures in the presence of a chiral tartrate counterion.[26,27] This self-assembly system is extremely versatile and shows rich polymorphism (twisted ribbons and helical ribbons).[28] Our previous work has shown that these nanostructures can be successfully transcribed to silica through sol−gel polycondensation with tetraethoxysilane (TEOS), leading to the formation of chiral silica nanoribbons[29] The morphology (periodicity and shape) of these inorganic nanoribbons can be precisely controlled by adjusting parameters such as organic gel concentration, gel aging time, and temperature of transcription, resulting in nanometric silica ribbons with finely controlled shape and size.[29] We herein investigate these silica nanoribbons by grafting them with RGD adhesive peptide to create biomimetic materials of the ECM, focusing in particular on the dimensions and the periodicity of these nanostructures. Our objective is to probe the role of altered periodicity, shape, and dimension in an ECM mimetic nanoscale matrix toward dictating the stem cell fate. To achieve this objective, helical silica nanoribbons with variable periodicities were accessed from the same native organic self-assembled helical nanoribbons, depending on gel aging time, between nanohelices with periodicity 63 ± 5 nm and twisted silica ribbons with larger periodicity (100 ± 15 nm). These silica nanoribbons were functionalized with RGD, then covalently grafted on activated glass substrates, and the effects of these disordered nanoribbon matrices (twisted ribbons *vs* helical ribbons) on stem cell adhesion and commitment toward specific cell lineage in the absence of supplements were investigated. The advantage of using Gemini self-assemblies is that it allows access to a diverse range of chiral silica nanostructures.[29] This system thus provides us the method to probe the cell−material interactions in a disordered nanoscale matrix, as a function of the periodic structure of these nanoribbons.

RESULTS

We have used the self-assembled organic template of 16−2−16 L-tartrate to produce twisted and helical silica nanoribbons with two different periodicities.[28] A 1 mM aqueous solution of 16−2−16 L-tartrate self-assembles to form helical nanoribbons within 1 day (Figure 1A). We have previously shown that these helical organic structures, when aged shortly, can partially unfold during silica polycondensation with TEOS, leading to twisted silica nanoribbons of increased periodicity.[28] Using this unique property of our self-assembly system, we have compared helical silica nanoribbons (periodicity: 63 ± 5 nm, Figure 1D,E) with twisted silica nanoribbons (Figure 1B,C) with increased periodicity (100 ± 15 nm) obtained from organic nanohelices aged for 20 days and 1 day, respectively. These silica nanoribbons were covalently functionalized with a cell adhesion peptide (containing an "RGD" sequence) in order to mimic *in vivo* ECM and promote specific cell−nanoribbon interactions.

Here, we shall discuss the functionalization protocol of the silica nanoribbons in general and their subsequent covalent grafting on activated glass substrates. This protocol was used for both helical and twisted silica nanoribbons.

The nanoribbons were first reacted with (3-aminopropyl)-triethoxysilane (APTES) in order to introduce $-NH_2$ groups on the surface of these ribbons (details in Materials and Methods section). Successful modification of the silica surface was established by the ninhydrin test, where the amine−ninhydrin complex showed UV−vis absorption at ∼600 nm (Figure 2C, black). The homogeneous distribution of the $-NH_2$ function on the silica surface was confirmed by homogeneous adsorption of citrate-stabilized Au nanoparticles on the amine-modified silica nanoribbons, through electrostatic interaction between the negatively charged citrate and the $-NH_3^+$ present on the silica surface (Figure 2B).[30] Reaction of the amine-modified silica with 3-(maleimido)propionic acid *N*-hydroxysuccinimide ester (SMP) introduced a reactive end group for subsequent covalent attachment through the cysteine end of an RGD sequence containing peptide. The disappearance of the absorption at 600 nm for the amine−ninhydrin complex confirmed the success of the reaction (Figure 2C, red), showing the absence of

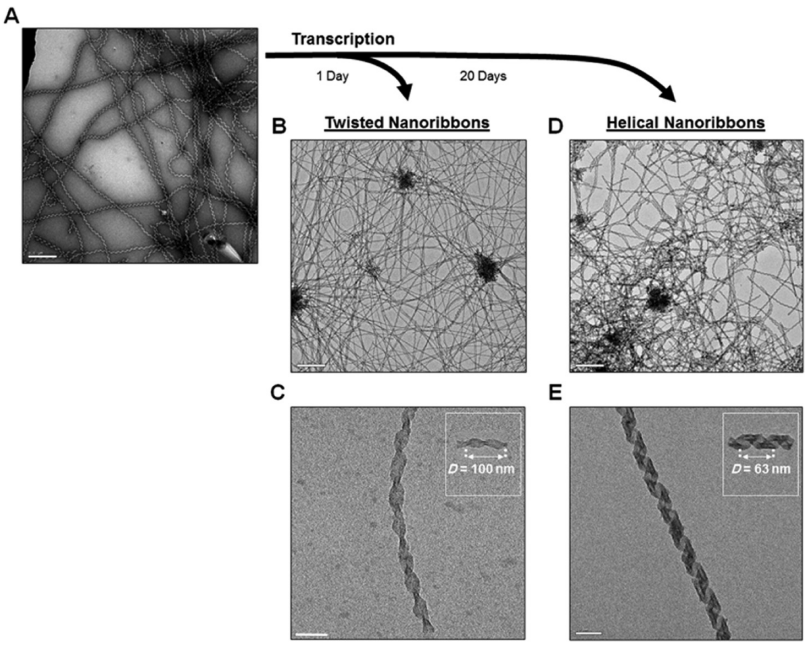

Figure 1. (A) TEM image of organic helical nanoribbons obtained from a 1 mM gel of 16−2−16 L-tartrate aged for 24 h, and (insets) results of silica transcription after different aging time. TEM images of silica nanoribbons: (B and C) twisted nanoribbons; (D and E) helical nanoribbons. The scale bars correspond to 500 nm in A, B, and D; 50 nm in C and E.

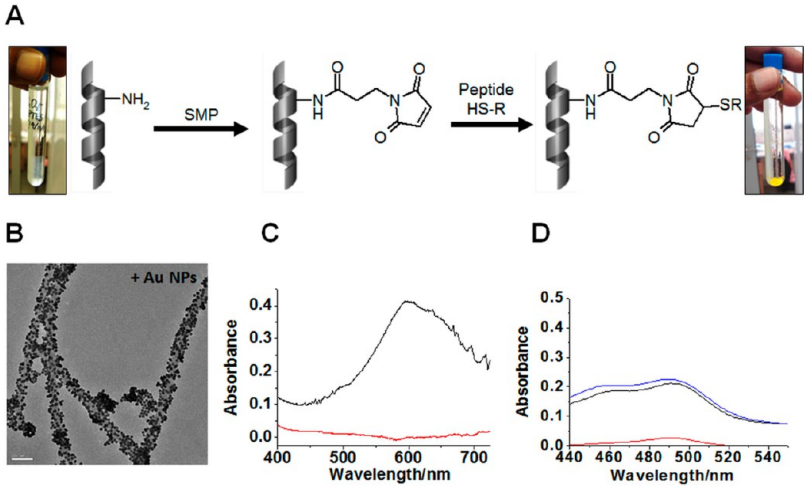

Figure 2. (A) Schematic chemical representation of covalent immobilization of fluorescent RGD-peptide on silica helical nanoribbons. The photos show the appearance of silica before (left) and after (right) grafting with fluorescent peptide. (B) TEM image of amine-modified silica helical nanoribbons, after treatment with citrate-stabilized Au NPs. (C) Absorption spectra after treatment of silica nanoribbon dispersion with ninhydrin, with amine-modified silica (black) and SMP-modifed silica (red). (D) Absorption spectra of fluorescent RGD-peptide-grafted silica nanoribbons (black: after treatment with 0.3 mM RGD-peptide solution; blue: after treatment with 1.3 mM RGD-peptide solution), and wash solvent (red).

free $-NH_2$ groups on the surface of the SMP-treated nanoribbons.

For covalent grafting of functional peptides on the silica nanoribbons, a cysteine-containing fluorescent peptide, FITC-KRGDSPC, was chosen. The peptide has the sequence RGD, which is present in many ECM proteins that take part in focal adhesion.[31] The peptide was also labeled with FITC (fluorescein isothiocyanate), to be able to investigate the silica nanoribbons (modified with RGD-peptide) grafted on a substrate through fluorescence microscopy. The grafting of this peptide onto the functionalized silica nanoribbons was accomplished by reacting an aqueous solution of the peptide with the SMP-modified aqueous silica dispersion (final concentration of the peptide: 0.3 mM; details in Materials and Methods section). The color of the silica turned yellow at the end of the process (Figure 2A, optical image, right; and Figure 3B), providing visual proof of the successful attachment of the peptide onto the nanoribbons. The UV−vis spectroscopy of the aqueous dispersion of these silica nanoribbons showed strong absorption attributed to the fluorescein chromophore

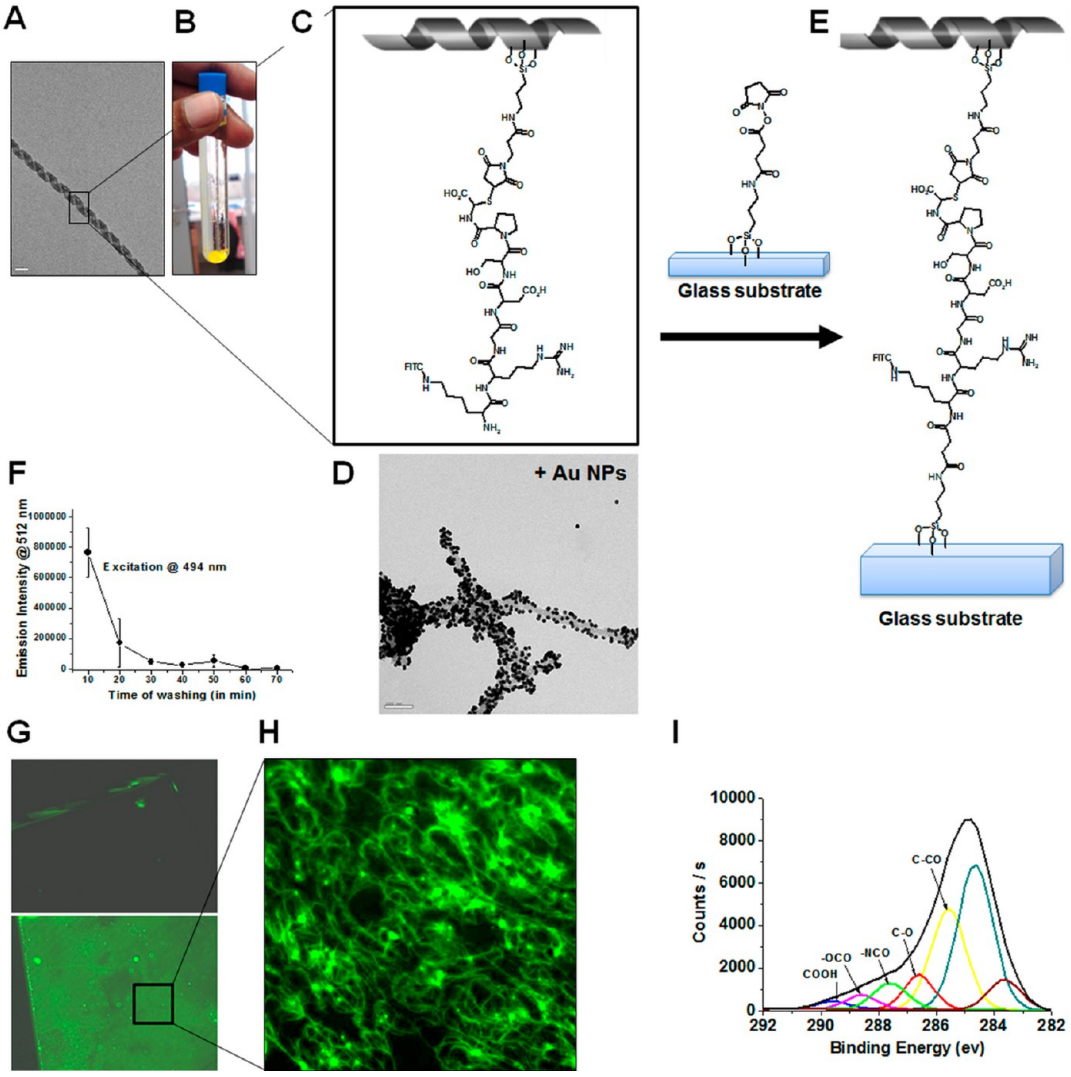

Figure 3. FITC-KRGDSPC peptide-modified silica helical nanoribbons: (A) TEM image (scale bar: 50 nm), (B) optical image under visible light, (C) schematic representation. (D) TEM image of peptide-modified silica helical nanoribbons, after treatment with citrate-stabilized Au NPs (scale: 100 nm). (E) Functionalized glass modified with the peptide-appended silica helical nanoribbons. (F) Fluorescence of wash liquid (excitation @ 494 nm); after each 10 min of sonication with 1 mL of Milli-Q water, fluorescence of the water was checked. (G) Fluorescence microscopy images (2.5× at excitation 488 nm) of control glass substrate (top) and functionalized glass substrate (bottom), after treatment with fluorescent peptide modified silica helical nanoribbons, followed by washing with water. (H) Fluorescence microscopy of fluorescent silica nanoribbon modified glass substrate at high magnification (40×). (I) C 1s XPS spectra of functionalized glass modified with peptide-appended silica helical nanoribbons.

(FITC) of the peptide (Figure 2D, black and blue), suggesting that the peptide is indeed grafted on the nanoribbons. After repeated washings of the peptide-modified silica with water (sonication, followed by centrifugation) to remove excess, unreacted peptide, the wash liquid became colorless (Figure 2D, red). Considering the fact that the free peptide is highly soluble in water, this result confirmed that the fluorescent peptide is covalently attached to the silica nanoribbons and not merely adsorbed on the nanoribbon surface. TEM image of the peptide-modified silica nanoribbons showed that the ribbon structure was preserved after functionalization (Figure 3A). Citrate-stabilized Au NPs were used as markers (*vide supra*) to demonstrate the presence of $-NH_2$ (available now at the N-terminus of the covalently attached peptide) on the silica nanoribbon surface (Figure 3D).[29,30] In order to confirm if the loading of peptides on the silica nanoribbons is optimal, *i.e.*, if the ribbon surface is saturated with the peptide, the reaction of the peptide with SMP-modified silica was repeated at 4 times higher concentration of peptide (1.3 mM). The peptide-modified silica thus obtained showed a similar absorbance intensity (Figure 2D, blue) to that observed after reaction with 0.3 mM peptide solution (Figure 2D, black), confirming that the silica nanoribbon surface is indeed saturated with peptide molecules.

The glass substrates were functionalized following the scheme shown in Figure S1 (details in Materials and Methods section). Briefly, (1) the precleaned (cleaned

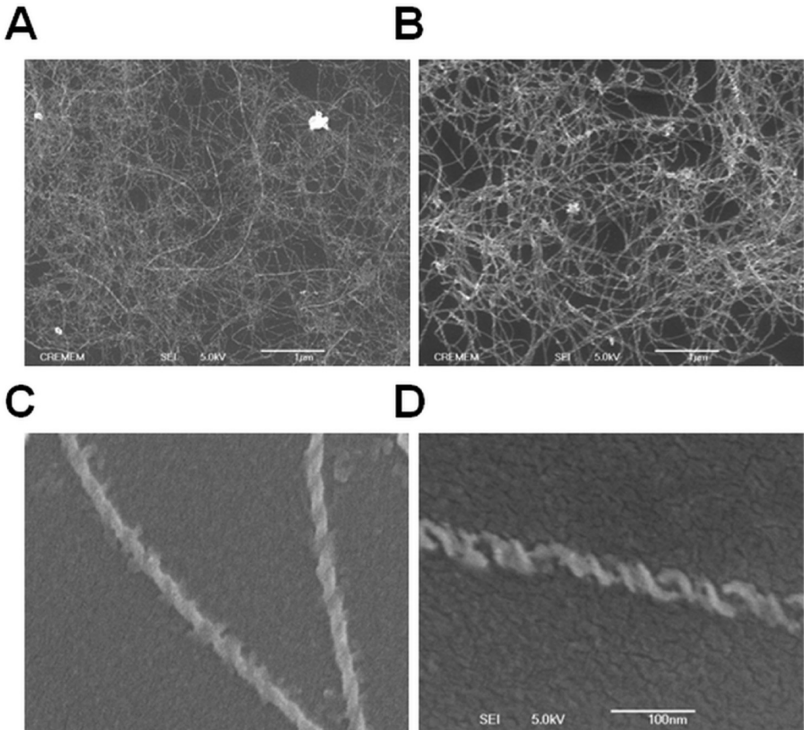

Figure 4. SEM images of functionalized glass substrates modified with peptide-attached silica nanoribbons: (A) twisted nanoribbons, (B) helical nanoribbons, (C and D) magnified images of covalently grafted twisted and helical nanoribbons. The scale bars correspond to (A) 1 μm, (B) 1 μm, and (C and D) 100 nm.

with piranha solution) glass substrate was treated with APTES to functionalize the surface with $-NH_2$. (2) The amine-functionalized substrate was then reacted with succinic anhydride to expose a carboxylic acid function on the surface. (3) Glass surface activation (for grafting of peptide-modified silica nanoribbons) was achieved by reaction with *N*-hydroxysuccinimide. The glass surface, before and after functionalization, was investigated by X-ray photoelectron spectroscopy (XPS) to confirm the success of the functionalization steps. The results of XPS experiments are summarized in Table S1. After step 1 (amine modification step), the appearance of N (0% to ~1.6%) demonstrated successful modification. Similarly, the N content expectedly increased (~1.6% to 3.2%) after step 3. The ratio (−NCO/COOH) also increased (Figure S2), demonstrating the success of glass activation.

The inorganic silica nanoribbons functionalized with the fluorescent peptide FITC-KRGDSPC were grafted on activated glass substrates from their aqueous dispersion. After the completion of the reaction (24 h), the glass substrates were washed repeatedly with water to remove excess, unreacted peptide (fluorescence spectroscopy, Figure 3F). Fluorescence microscopy image of functionalized glass with covalently attached fluorescent silica nanoribbons showed the presence of peptide even after washing (Figure 3G, bottom), as opposed to the control glass, which did not show any fluorescence (Figure 3G, top). At high magnification, the presence of fluorescent silica nanoribbons on the glass substrate was clearly evident (Figure 3H). XPS investigation of the nanoribbon-modified glass substrate expectedly showed the presence of peaks corresponding to NCO and COOH in the C 1s spectrum (Figure 3I). These experiments confirm that the covalent grafting of fluorescent peptide modified silica nanoribbons on activated glass substrates was successful. Further confirmation to this end was obtained from scanning electron microscopy (SEM) analysis of the silica nanoribbon modified glass substrates, which showed the presence of chiral silica nanoribbons even after rigorous washing of the substrate (Figure 4A and B). A magnified SEM image revealed that the nanoribbon structure was not affected after covalent grafting (helical nanoribbon modified substrate, Figure 4C). Semiquantitative fluorescence microscopy analysis of these glass substrates confirmed similar RGD peptide density in the helical ribbon and twisted ribbon modified substrates (Figure S3).

In order to study the unique influence of nanoribbon shape and periodicity on the behaviors of stem cells, all cell adhesion experiments were carried out without any serum for the first 8 h of culture. Glass substrates with smooth surfaces without any functionalization and those homogeneously functionalized with RGD peptides (FITC-KRGDSPC) were used as reference surfaces and compared with glass surfaces on which RGD-functionalized nanoribbons (twisted and helical nanoribbons) are grafted. SEM images of human mesenchymal stem cells (hMSCs) cultured for 4 h (without serum) on the surface modified with RGD helical or twisted nanoribbon revealed significant differences in

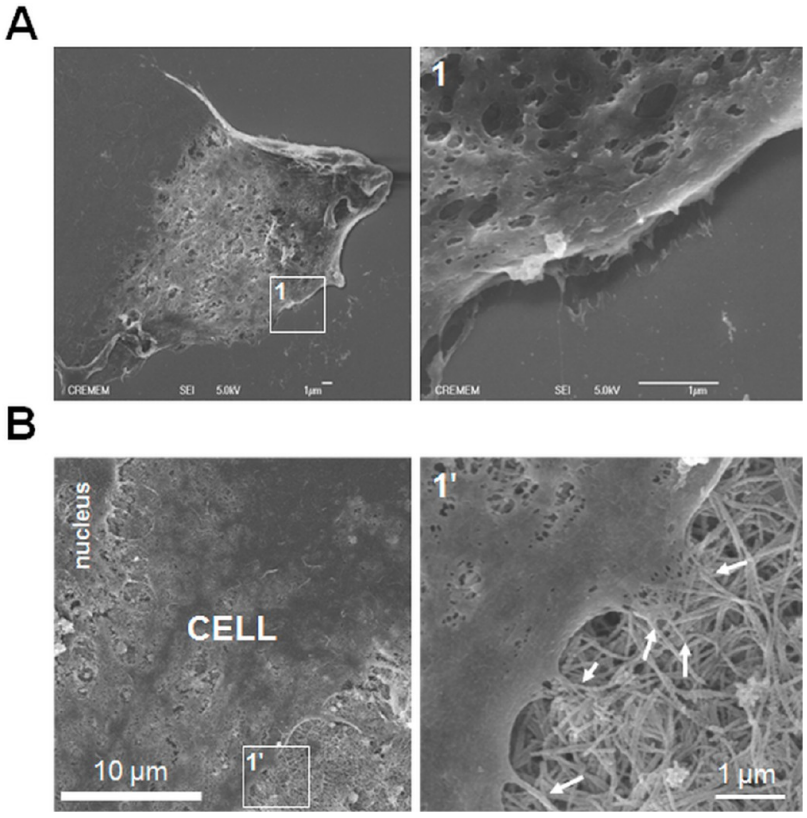

Figure 5. (A) SEM images of hMSCs on control glass substrates and (B) on glass substrates grafted with helical nanoribbon-RGD after 4 h of culture. (1 and 1′) Magnified SEM images of cell−substrate nanoscale interactions. hMSCs become progressively more spread out and have small cell extensions (filopodia-like structures) on glass substrates grafted with helical nanoribbon-RGD (see white arrows in 1′).

stem cell adhesion and cell shape in comparison with control substrates. This was also confirmed by the fluorescence micrograph (Figure S4A). Filopodia quantification per cell confirms this observation (Figure S4B). Furthermore, as shown in Figure 5 and Figure S5 (white arrows), we clearly see the presence of small filopodia extensions for glass grafted with both twisted and helical nanoribbon-RGD, whereas for control surfaces, these filopodia extensions vanish. After 24 h of culture, the surfaces functionalized with nanohelical ribbons (periodicity ~63 nm) induces more stable hMSC cell adhesion and better cell spread (Figure S6) than other conditions (control surfaces and surfaces functionalized with twisted nanoribbons). Indeed, interestingly, many fibrillar focal adhesions (FAs) were observed on hMSCs cultured on glass substrates grafted with helical nanoribbon-RGD (Figure 6A). In addition, FA size quantification showed an important difference between nanohelical conditions with respect to other conditions; that is, both control surfaces as well as the surface grafted with twisted nanoribbons, the size of FAs being significantly higher in the former (Figure 6B). However, the surface with twisted nanoribbon-RGD shows a lower presence of fibrillar FAs compared to the surface with helical nanoribbon-RGD but higher than control surfaces (Figure 6).

Finally, hMSC behavior on grafted helical nanoribbon-RGD resulted in a preferential differentiation into osteogenic lineage after 96 h of incubation, which was confirmed by immunofluorescence staining of three common protein osteogenic markers:[32,33] STRO-1 (stem cell marker), osterix (Osx, a transcriptional factor induced by Runx2, which is required for the differentiation of osteoprogenitor cells into functional osteoblasts), and osteopontin (OPN). We show clearly a decrease of STRO-1 marker in the helical nanoribbon-RGD condition (Figure 7A). However, STRO-1 is present in control conditions and in the twisted nanoribbon-RGD condition (Figure 7A). Moreover, Osx is more expressed in hMSCs cultured on helical nanoribbon-RGD (Figure 7B). We observe a low expression on twisted nanoribbon-RGD and the absence of expression in control conditions. OPN is expressed only in helical nanoribbon-RGD conditions and not in the other conditions (Figure 7C).

DISCUSSION

These results clearly demonstrate the strong effect of silica nanohelices grafted on glass surfaces on the adhesion and differentiation behaviors of hMSCs. The differences of the behaviors of hMSCs on the surfaces with helical nanoribbons and twisted nanoribbons are intriguing. The twisted silica nanoribbons used in this work are a structural variant of the helical silica nanoribbons originated from the same organic template. Twisted organic nanoribbons having larger periodicities

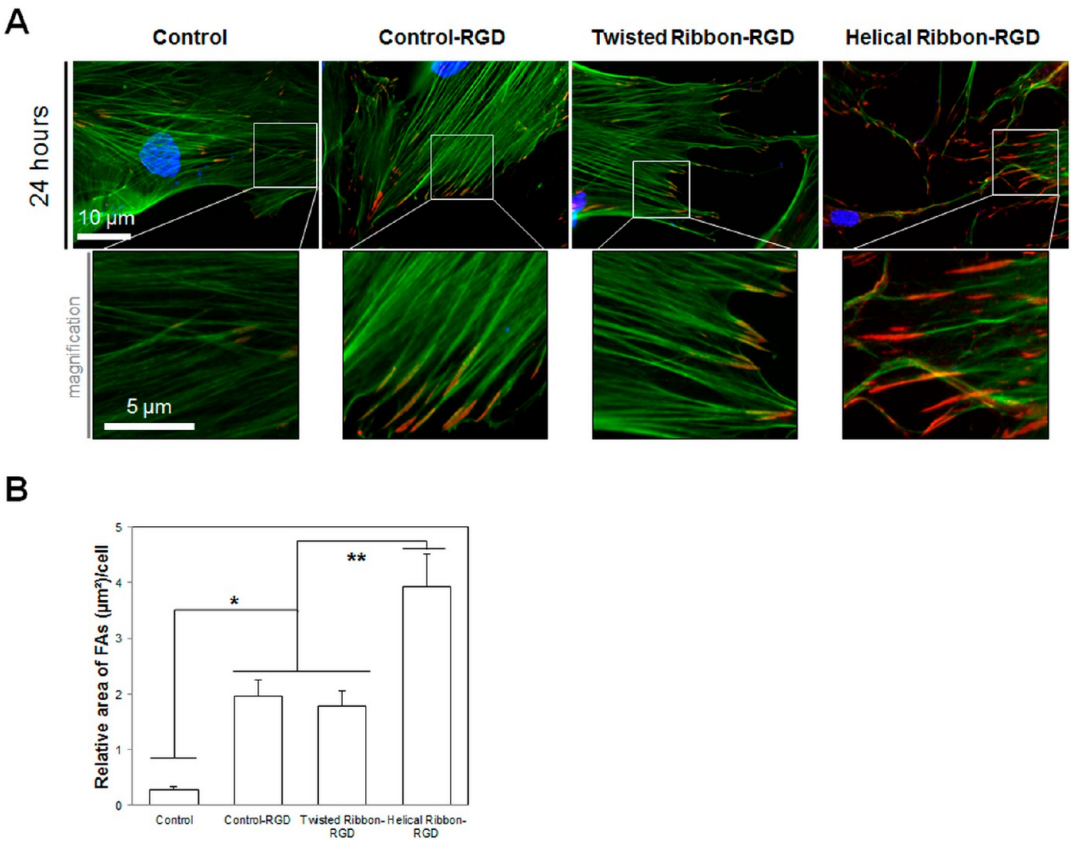

Figure 6. (A) After 24 h of seeding, focal contact formation and stress fiber assembly were shown on different glass modified substrates as demonstrated by antivinculin staining (red), phalloidin staining (green), and DAPI (blue). (B) Relative area of focal adhesion contacts on control glass substrates and control glass substrates grafted with RGD, twisted nanoribbon-RGD, and helical nanoribbon-RGD ($p < 0.01$, *$p < 0.001$).**

are generated by partial unfolding and stress redistribution of the corresponding helical nanoribbons, which can be effectively viewed as the stretching of the helical nanoribbons.

These results have significant implications for understanding both chemical and physical effects of the *in vivo* ECM microenvironment. Several critical questions thus arise: how do the stem cells interpret the periodicity on the nanoribbons? In other words, by which signaling pathway is the differentiation dictated? It is already described in the literature that, for example, stem cells sense microenvironment elasticity by myosin II among others.[3,6] Among the cell's cytoskeletal motors, myosin II isoforms are implicated in tensioning cortical actin structures.[34] These actin structures are in turn linked to FA complexes that provide the pathway of force transmission from inside the cell to the elastic matrix. These complexes are well-known signaling molecules that are well placed to act as the mechanotransducers.[34] Interestingly, hMSCs incubated in helical nanoribbon-RGD conditions for 96 h of culture in pharmacological agent for targeting nonmuscle myosin II inhibition (Blebbistatin) were not differentiated into osteoblast-like cells (Figure S7). The osteogenic commitment was inhibited (Figure S7B). STRO-1 was present in all conditions (Figure S7A). These results show that the way the cells interpret the helical periodicity is myosin II dependent, similar to the mechanism by which the cells sense the elasticity of their microenvironment. Future experiments should be performed in order to further test the eventual similarity between these mechanisms.

One of the important interactions of the cell with its surrounding environment is the focal adhesion, which is governed by the binding of integrin transmembrane proteins with ligands in the ECM.[35] These interactions dictate the cell behaviors, such as adhesion, spreading, and directed differentiation of stem cells into specific cell lineages.[4,6] Our programmed synthetic ECM systems elucidate intriguing aspects of these complex cell–ECM nanoscale interactions and unravel their roles in the diverse responses of the cells. Our results clearly demonstrate that stem cell fate is strongly linked to nanoperiodicity and nanoscale dimensions. Indeed, we show that it is possible to induce fibrillar focal adhesion and thus to direct the commitment of stem cells to osteoblast lineage solely by altering the periodicity and dimension (shape and size) of the highly organized nanoribbons (twisted nanoribbons *vs* helical nanoribbons, Figure 1) and that the cells sense this nanoperiodicity in the same way they respond to the elasticity of the ECM microenvironment.

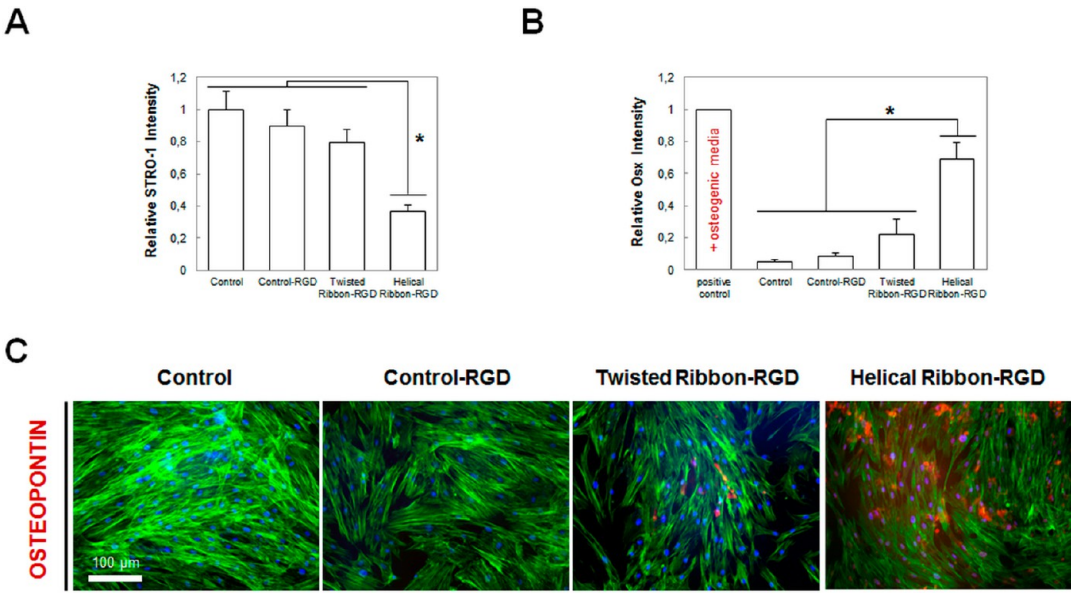

Figure 7. (A and B) Total cellular STRO-1 and Osx immunofluorescence intensity was quantified for hMSC cultured during 96 h on different glass modified substrates (*$p < 0.005$). Positive control consists of hMSCs cultured on glass substrates in osteogenic media (see Materials and Methods section). (C) Immunofluorescent staining for OPN (red), actin (green), and nucleus (blue) in hMSCs on different glass modified substrates during 96 h. hMSCs are committed into osteoblast lineage on glass substrates grafted with helical nanoribbon-RGD.

This suggested mechanism is in agreement with the general notion that when the stem cells are stressed and have mature focal contacts (here, fibrillar FAs), they tend to differentiate into an osteoblast lineage.[1,3,6,10,13] We have observed fibrilar adhesions in the case of hMSCs seeded on helical nanoribbons. Fibrillar adhesions represent the end point in terms of adhesion maturation. Their association with large stable NMII-decorated actin filament bundles results in large adhesions with a lifetime of several hours, and this class of adhesions has an active role in organizing the ECM. These results reveal important insights into the mechanism and scope of these interactions in the biological environment and to what extent they can be modulated in synthetic matrices to achieve a predictable control over the cell response in the context of engineered regenerative biomaterials.

Considering the fact that great strides are being made in utilizing peptide-based 3D hydrogel matrices with biologically active peptide sequences to encapsulate cells and promote and control a multitude of cell responses,[36] the present result on the influence of periodicity and nanoscale shape on the 2D surface in dictating stem cell fate is expected to open up exciting avenues in this field. Indeed, expanding our study to hydrogel materials with a 3D scaffold with nanohelices with controlled nanometric periodicity represents a promising concept for bone tissue engineering.

CONCLUSION

The identification of mechanisms that direct adult hMSC osteogenic differentiation is of prime interest for developing therapeutic strategies to promote bone formation and repair. In this study, we established the essential role of nanoribbon shape and periodicity in hMSC commitment and showed that helical nanoribbons with a specific periodicity of ~60 nm induce much more specific cell adhesion through the fibrillar FA formation and stronger commitment of cells into osteoblast lineage than twisted nanoribbons with a periodicity of ~100 nm. We documented that inhibition of non-muscle myosin II with blebbistatin is sufficient to block this osteoblast commitment, demonstrating that stem cells interpret the nanohelical shape and periodicity microenvironment physically. This system closely models the ECM structural changes that happen due to mutations during induction of several life-threatening diseases. The present study also provides a tool to promote hMSC osteogenic capacity, which may be exploited in a 3D scaffold for bone tissue engineering and repair.

MATERIALS AND METHODS

Synthesis of 16−2−16 L-Tartrate. The 16−2−16 gemini amphiphile with L-tartrate counterions was synthesized following our previously reported procedure.[37]

Preparation of Silica Helical Nanoribbons and Twisted Nanoribbons. The 1 mM aqueous gels of 16−2−16 L-tartrate were aged for an adequate time (24 h for transcription to twisted silica nanoribbons and 20 days for transcription to helical silica nanoribbons), then were used as organic templates to prepare silica nanostructures through sol−gel polycondensation. Typically, 0.5 mL of 5 wt % tetraethoxysilane was prehydrolyzed in water (pH 6) for 12 h at room temperature and then added to 0.5 mL of the

appropriately aged gel. The reaction mixture was vortexed (2000 rpm) for a few seconds and then kept at 20 °C for 48 h. The samples were then washed thoroughly with ethanol to remove excess TEOS and all organic components. The helical silica nanoribbons obtained by this process had a diameter of 35 ± 5 nm and a periodicity of 63 ± 5 nm. The corresponding twisted silica nanoribbons showed a diameter of 20 ± 3 nm and a periodicity of 100 ± 15 nm.

Covalent Modification of Silica Nanoribbons with RGD Peptides. *Modification with APTES.* A 1 mL amount of the silica nanoribbon dispersion in ethanol (obtained from the previous step) was treated with 50 μL of 1% (3-aminopropyl)triethoxysilane (10 μL of APTES in 1 mL of ethanolic solution), sonicated for 5 min, and then heated at 70 °C (oil bath) overnight. The samples were then thoroughly washed with ethanol.

Reaction with SMP. To 1 mL of the silica nanoribbon dispersion in ethanol (obtained after APTES modification), 1 mL of an ethanolic dispersion of 3-(maleimido)propionic acid *N*-hydroxysuccinimide ester (3 mg) was added. The reaction mixture was sonicated for 3 h and then washed thoroughly with water.

Reaction with Fluorescent Peptide. To 1 mL of an aqueous silica nanoribbon dispersion (obtained after SMP modification), a 1 mL aqueous solution of FITC-KRGDSPC (0.3 mM) was added. The reaction mixture was sonicated for 5 min and then kept on a roller/mixer (30 rpm) in the dark for 24 h. The sample was washed several times with water, until the wash liquid became colorless.

Activation of Glass Substrates. *Reaction with APTES (ref 38).* The glass substrate was washed with piranha solution, followed by water, dried in an oven at 100 °C for 12 h, and then inserted in the glovebox. First, the substrate was heated at 150 °C under vacuum (10^{-5} Torr) for 18 h. Then, it was immersed in 2 mL of a 10 mM hexane solution of APTES and shaken at 200 rpm under an Ar atmosphere for 2 h. The substrate was then cleaned by two rinsings with dry hexane (0.5 h each), followed by a third rinsing overnight. The washed glass substrate was heated at 100 °C under vacuum (10^{-5} Torr) for 4 h.

Reaction with Succinic Anhydride (SA). The glass substrate was immersed in 2 mL of a DMF solution of SA (4 mg) and shaken under an Ar atmosphere for 3 h. The substrate was then washed by three rinsings with DMF (0.5 h each), followed by a fourth rinsing overnight. The glass substrate was heated at 100 °C under vacuum (10^{-5} Torr) for 4 h.

Reaction with N-Hydrioxysuccinimide (NHS). The glass substrate was immersed in a 3 mL of an aqueous solution consisting of 1-ethyl-3-(3-dimethylaminopropyl)carbodiimide (172 mM), NHS (104 mM), and MES buffer (94 mM) and kept at 4 °C for 20 h. The substrate was washed with water several times by shaking (200 rpm).

Covalent Grafting of RGD-Modifed Silica Nanoribbons on Functionalized Glass Substrates. The silica nanoribbons functionalized with the fluorescent peptide FITC-KRGDSPC were dispersed in water, and 2 mL of this suspension (0.2 mg of silica/mL) was added to a container with the activated glass substrates. Under this condition, the substrates were immersed in the water suspension of the peptide-modified silica nanoribbons. The reaction system was allowed to stand in the dark at room temperature for 24 h. Afterward, the glass substrates were sonicated with 1 mL of water (replacing the water with fresh water every 10 min) for 1 h, in order to remove excess, unreacted silica nanoribbons from the glass surface.

Characterization of Chemical Grafting. The surfaces were characterized using three methods:

X-ray Photoelectron Spectroscopy[39] *for Chemical Characterization of the Glass Surface Grafted with Twisted and Helical Nanoribbons.* To do this, a VG Scientific ESCALAB photoelectron spectrometer was used for the surface analysis with a nonmonochromatized Mg K 1253.6 eV source of 100 W. The area of the analytical X-ray spot on the sample surface was about 250 μm. We used a 45° insert angle that corresponds to 3−5 nm of analyzed depth. A flood gun was used for charge compensation. Acquisition of high-resolution spectra was done at a constant pass energy of 20 eV.

Fluorescent Microscopy of Labeled Peptides (refs 40−42*).* Fluorescence microscopy of grafted labeled peptides (Leica microsystem DM5500B, microscope with a motorized, programmable stage using a CoolSnap HQ camera controlled by Metamorph 7.6) was used to confirm a uniform peptide grafting. Mimetic peptides of adhesion proteins were linked to FITC fluorochrome (FITC-KRGDSPC). FITC fluorochrome was linked in a covalent way at the N terminal of the peptide. Image J software (NIH, http://rsb.info.nih.gov/ij/) was used to quantify the relative fluorescent intensity of the grafted mimetic peptides.

Scanning Electron Microscopy. Direct observations of glass substrates grafted with nanometric twisted ribbons and helical ribbons were performed. Samples were gold-coated for 10 s and observed with a scanning electron microscope (Hitachi S2500) at 10 kV. SEM analysis of the silica nanoribbon-grafted glass substrates revealed the presence of nanoribbons everywhere on the glass surface, with some variation of the density of nanoribbons. Quantification from the SEM images of the nanoribbons grafted on the glass substrates revealed the presence of ∼90−95% helical/twisted nanoribbons in the respective substrates grafted with helical and twisted nanoribbons. For example, for the glass substrates grafted with helical nanoribbons, SEM quantification revealed the presence of 96% helical nanoribbons and 4% twisted nanoribbons, and *vice versa*.

Cell Culture. Primary human (bone marrow) mesenchymal stem cells were obtained from LONZA (Switzland, cat. no. PT-2501). Cells were cultured in minimum essential medium (Alpha-MEM, Gibco) supplemented with 10% (v/v) FBS and 1% penicillin/streptomycin and incubated in a humidified atmosphere containing 5% (v/v) CO_2 at 37 °C. All cell culture experiments were carried out without any serum for the first 8 h of culture. All cells were used at low passage numbers (passage 2 to 4), were subconfluently cultured, and were seeded at 10^4 cells/cm^2 for experiments. The pharmacological agent blebbistatin (Sigma, France) was employed at 1 μM. hMSCs were exposed to blebbistatin for 1 h after seeding on materials each 24 h during 3 days.

Scanning Electron Microscopy. Initially cells were seeded on the substrates at a density of 1×10^4 cells/mL. After 4 h of culture (serum free), cells were washed with PBS 1× and then fixed with paraformaldehyde in PBS (4%) during 20 min at 4 °C. Samples were dehydrated in increasing concentrations of ethanol (30, 70, 80, 90, 95, and 100%) and critical point dried. Replicas were gold-coated for 10 s and observed with a scanning electron microscope (Hitachi S2500) at 10 kV.

Immunostaining. After 4, 24, and 96 h of culture, the cells on the surfaces were fixed for 20 min in 4% paraformaldehyde/PBS at 4 °C. After fixation, the cells were permeabilized in a PBS solution of 1% TritonX100 for 15 min. Cell cytoskeletal filamentous actin (F-actin) was visualized by treating the cells with 5 U/mL Alexa Fluor 488 phalloidin (Sigma, France) for 1 h at 37 °C. Vinculin was visualized by treating the cells with 1% (v/v) monoclonal antivinculin (clone hVIN-1 antibody produced in mouse) for 1 h at 37 °C. Then we coupled with Alexa Fluor 568 ($F(ab')_2$ fragment of rabbit anti-mouse IgG(H + L)) during 30 min at room temperature. After 96 h, osterix was visualized by treating the cells with 1% (v/v) monoclonal anti-osterix (antibody produced in rabbit) for 1 h at 37 °C. Then we coupled with Alexa Fluor 568 ($F(ab')_2$ fragment of mouse anti-rabbit IgG(H + L)) during 30 min at room temperature. OPN was visualized by treating the cells with 1% (v/v) monoclonal anti-OPN (Abcam, Cambridge), for 1 h at 37 °C. Then we coupled with Alexa Fluor 588 ($F(ab')_2$ fragment of goat anti-rabbit IgG(H+L)) for 30 min at room temperature. No detection of neuronal cytoskeletal marker β3 tubulin (stained by anti-β3 tubulin (Sigma, France)) and muscle transcription factor MyoD1 (stained with anti-MyoD1 (Santa Cruz Biotechnology, USA)) was observed on hMSCs cultured on different surfaces during 1 week (results not shown).

For quantification of STRO-1, Osx and vinculin (focal adhesions) positive contacts' number and areas, we used the freeware image analysis Image J software.[14,39,41−43] We opened the raw image, converted it to an 8-bit file, and used the unsharp mask feature (settings 1:0.2) before removing the image background (rolling ball radius 10). After smoothing, the resulting image, which appears similar to the original photomicrograph but with minimal background, was then converted to a binary image by setting a threshold. Threshold values were determined

empirically by selecting a setting that gave the most accurate binary image for a subset of randomly selected photomicrographs with varying glass substrates. The cell area was determined by manual delineation on raw fluorescent images; total contact focal area and mean contact area per cell were calculated by "analyse particules" in Image J. A minimum of 20 to 30 cells per condition were analyzed.

Statistical Analysis. In terms of fluorescence assay, all data was expressed as mean ± standard error and analyzed statistically by the paired Student's *t* test method. Significant difference was determined at p values at least <0.01.

Conflict of Interest: The authors declare no competing financial interest.

Supporting Information Available: Figures S1−S7, Table S1. This material is available free of charge *via* the Internet at http://pubs.acs.org.

Acknowledgment. The authors thank Dimytro Dedovets for technical assistance and stimulating discussions. We also thank Michel Martineau at CREMEM, Université Bordeaux 1, for recording SEM images. This work was supported by the "Région Aquitaine", the GIS "Advanced Materials in Aquitaine", as well as the "Agence Nationale pour la Recherche" (ANR).

REFERENCES AND NOTES

1. Discher, D. E.; Mooney, D. J.; Zandstra, P. W. Growth Factors, Matrices, and Forces Combine and Control Stem Cells. *Science* **2009**, *324*, 1673–1677.
2. Huebsch, N.; Mooney, D. J. Inspiration and Application in the Evolution of Biomaterials. *Nature* **2009**, *462*, 426–432.
3. Engler, A. J.; Sen, S.; Sweeney, H. L.; Discher, D. E. Matrix Elasticity Directs Stem Cell Lineage Specification. *Cell* **2006**, *126*, 677–689.
4. Huebsch, N.; Arany, P. R.; Mao, A. S.; Shvartsman, D.; Ali, O. A.; Bencherif, S. A.; Rivera-Feliciano, J.; Mooney, D. J. Harnessing Traction-Mediated Manipulation of the Cell/Matrix Interface to Control Stem-Cell Fate. *Nat. Mater.* **2010**, *9*, 518–526.
5. Dalby, M. J.; Gadegaard, N.; Tare, R.; Andar, A.; Riehle, M. O.; Herzyk, P.; Wilkinson, C. D.; Oreffo, R. O. The Control of Human Mesenchymal Cell Differentiation Using Nanoscale Symmetry and Disorder. *Nat. Mater.* **2007**, *6*, 997–1003.
6. Zouani, O. F.; Kalisky, J.; Ibarboure, E.; Durrieu, M. C. Effect of Bmp-2 from Matrices of Different Stiffnesses for the Modulation of Stem Cell Fate. *Biomaterials* **2013**, *34*, 2157–2166.
7. Sargeant, T. D.; Aparicio, C.; Goldberger, J. E.; Cui, H.; Stupp, S. I. Mineralization of Peptide Amphiphile Nanofibers and Its Effect on the Differentiation of Human Mesenchymal Stem Cells. *Acta Biomater.* **2012**, *8*, 2456–2465.
8. Rajangam, K.; Behanna, H. A.; Hui, M. J.; Han, X.; Hulvat, J. F.; Lomasney, J. W.; Stupp, S. I. Heparin Binding Nanostructures to Promote Growth of Blood Vessels. *Nano Lett.* **2006**, *6*, 2086–2090.
9. Sargeant, T. D.; Guler, M. O.; Oppenheimer, S. M.; Mata, A.; Satcher, R. L.; Dunand, D. C.; Stupp, S. I. Hybrid Bone Implants: Self-Assembly of Peptide Amphiphile Nanofibers within Porous Titanium. *Biomaterials* **2008**, *29*, 161–171.
10. Oh, S.; Brammer, K. S.; Li, Y. S.; Teng, D.; Engler, A. J.; Chien, S.; Jin, S. Stem Cell Fate Dictated Solely by Altered Nanotube Dimension. *Proc. Natl. Acad. Sci. U.S.A.* **2009**, *106*, 2130–2135.
11. Dalby, M. J.; McCloy, D.; Robertson, M.; Agheli, H.; Sutherland, D.; Affrossman, S.; Oreffo, R. O. Osteoprogenitor Response to Semi-Ordered and Random Nanotopographies. *Biomaterials* **2006**, *27*, 2980–2987.
12. Dalby, M. J.; McCloy, D.; Robertson, M.; Wilkinson, C. D.; Oreffo, R. O. Osteoprogenitor Response to Defined Topographies with Nanoscale Depths. *Biomaterials* **2006**, *27*, 1306–1315.
13. Park, J.; Bauer, S.; von der Mark, K.; Schmuki, P. Nanosize and Vitality: TiO_2 Nanotube Diameter Directs Cell Fate. *Nano Lett.* **2007**, *7*, 1686–1691.
14. Zouani, O. F.; Chanseau, C.; Brouillaud, B.; Bareille, R.; Deliane, F.; Foulc, M. P.; Mehdi, A.; Durrieu, M. C. Altered Nanofeature Size Dictates Stem Cell Differentiation. *J. Cell. Sci.* **2012**, *125*, 1217–1224.
15. Kshitiz; Kim, D. H.; Beebe, D. J.; Levchenko, A. Micro- and Nanoengineering for Stem Cell Biology: The Promise with a Caution. *Trends Biotechnol.* **2011**, *29*, 399–408.
16. Kim, D. H.; Provenzano, P. P.; Smith, C. L.; Levchenko, A. Matrix Nanotopography as a Regulator of Cell Function. *J. Cell. Biol.* **2012**, *197*, 351–360.
17. Buxboim, A.; Ivanovska, I. L.; Discher, D. E. Matrix Elasticity, Cytoskeletal Forces and Physics of the Nucleus: How Deeply Do Cells `Feel' Outside and In? *J. Cell. Sci.* **2010**, *123*, 297–308.
18. Gautieri, A.; Vesentini, S.; Redaelli, A.; Buehler, M. J. Hierarchical Structure and Nanomechanics of Collagen Microfibrils from the Atomistic Scale Up. *Nano Lett.* **2011**, *11*, 757–766.
19. Kuivaniemi, H.; Tromp, G.; Prockop, D. J. Mutations in Collagen Genes: Causes of Rare and Some Common Diseases in Humans. *FASEB J.* **1991**, *5*, 2052–2060.
20. Ljunggren, O.; Lindahl, K.; Rubin, C. J.; Kindmark, A. Allele-Specific Gene Silencing in Osteogenesis Imperfecta. *Endocr. Dev.* **2011**, *21*, 85–90.
21. Marini, J. C.; Forlino, A.; Cabral, W. A.; Barnes, A. M.; San Antonio, J. D.; Milgrom, S.; Hyland, J. C.; Korkko, J.; Prockop, D. J.; De Paepe, A.; *et al*. Consortium for Osteogenesis Imperfecta Mutations in the Helical Domain of Type I Collagen: Regions Rich in Lethal Mutations Align with Collagen Binding Sites for Integrins and Proteoglycans. *Hum. Mutat.* **2007**, *28*, 209–221.
22. Rauch, F.; Glorieux, F. H. Osteogenesis Imperfecta. *Lancet* **2004**, *363*, 1377–1385.
23. Tedeschi, E.; Antoniazzi, F.; Venturi, G.; Zamboni, G.; Tato, L. Osteogenesis Imperfecta and Its Molecular Diagnosis by Determination of Mutations of Type I Collagen Genes. *Pediatr. Endocrinol. Rev.* **2006**, *4*, 40–46.
24. Vaziri, A.; Gopinath, A. Cell and Biomolecular Mechanics in Silico. *Nat. Mater.* **2008**, *7*, 15–23.
25. Gautieri, A.; Uzel, S.; Vesentini, S.; Redaelli, A.; Buehler, M. J. Molecular and Mesoscale Mechanisms of Osteogenesis Imperfecta Disease in Collagen Fibrils. *Biophys. J.* **2009**, *97*, 857–865.
26. Oda, R.; Huc, I.; Schmutz, M.; Candau, S. J.; MacKintosh, F. C. Tuning Bilayer Twist Using Chiral Counterions. *Nature* **1999**, *399*, 566–569.
27. Berthier, D.; Buffeteau, T.; Leger, J. M.; Oda, R.; Huc, I. From Chiral Counterions to Twisted Membranes. *J. Am. Chem. Soc.* **2002**, *124*, 13486–13494.
28. Oda, R.; Artzner, F.; Laguerre, M.; Huc, I. Molecular Structure of Self-Assembled Chiral Nanoribbons and Nanotubules Revealed in the Hydrated State. *J. Am. Chem. Soc.* **2008**, *130*, 14705–14712.
29. Delclos, T.; Aime, C.; Pouget, E.; Brizard, A.; Huc, I.; Delville, M. H.; Oda, R. Individualized Silica Nanohelices and Nanotubes: Tuning Inorganic Nanostructures Using Lipidic Self-Assemblies. *Nano Lett.* **2008**, *8*, 1929–1935.
30. Tamoto, R.; Lecomte, S.; Si, S.; Moldovan, S.; Ersen, O.; Delville, M.-H.; Oda, R. Gold Nanoparticle Deposition on Silica Nanohelices: A New Controllable 3D Substrate in Aqueous Suspension for Optical Sensing. *J. Phys. Chem. C* **2012**, *116*, 23143–23152.
31. Corti, A.; Curnis, F. Isoaspartate-Dependent Molecular Switches for Integrin-Ligand Recognition. *J. Cell. Sci.* **2011**, *124*, 515–522.
32. Karsenty, G. Transcriptional Control of Skeletogenesis. *Annu. Rev. Genomics Hum. Genet.* **2008**, *9*, 183–196.
33. Simmons, P. J.; Torok-Storb, B. Identification of Stromal Cell Precursors in Human Bone Marrow by a Novel Monoclonal Antibody, Stro-1. *Blood* **1991**, *78*, 55–62.
34. Zajac, A. L.; Discher, D. E. Cell Differentiation through Tissue Elasticity-Coupled, Myosin-Driven Remodeling. *Curr. Opin. Cell. Biol.* **2008**, *20*, 609–615.
35. Brown, A. E.; Discher, D. E. Conformational Changes and Signaling in Cell and Matrix Physics. *Curr. Biol.* **2009**, *19*, R781–789.

36. Wu, E. C.; Zhang, S.; Hauser, C. A. E. Self-Assembling Peptides as Cell-Interactive Scaffolds. *Adv. Funct. Mater.* **2012**, *22*, 456–468.
37. Brizard, A.; Aime, C.; Labrot, T.; Huc, I.; Berthier, D.; Artzner, F.; Desbat, B.; Oda, R. Counterion, Temperature, and Time Modulation of Nanometric Chiral Ribbons from Gemini-Tartrate Amphiphiles. *J. Am. Chem. Soc.* **2007**, *129*, 3754–3762.
38. Porte-Durrieu, M. C.; Labrugere, C.; Villars, F.; Lefebvre, F.; Dutoya, S.; Guette, A.; Bordenave, L.; Baquey, C. Development of Rgd Peptides Grafted onto Silica Surfaces: XPS Characterization and Human Endothelial Cell Interactions. *J. Biomed. Mater. Res.* **1999**, *46*, 368–375.
39. Chollet, C.; Chanseau, C.; Remy, M.; Guignandon, A.; Bareille, R.; Labrugere, C.; Bordenave, L.; Durrieu, M. C. The Effect of Rgd Density on Osteoblast and Endothelial Cell Behavior on RGD-Grafted Polyethylene Terephthalate Surfaces. *Biomaterials* **2009**, *30*, 711–720.
40. Zouani, O. F.; Chollet, C.; Guillotin, B.; Durrieu, M. C. Differentiation of Pre-Osteoblast Cells on Poly(ethylene terephthalate) Grafted with RGD and/or BMPs Mimetic Peptides. *Biomaterials* **2010**, *31*, 8245–8253.
41. Lei, Y.; Zouani, O. F.; Remy, M.; Ayela, C.; Durrieu, M. C. Geometrical Microfeature Cues for Directing Tubulogenesis of Endothelial Cells. *PLoS One* **2012**, *7*, e41163.
42. Lei, Y.; Zouani, O. F.; Rami, L.; Chanseau, C.; Durrieu, M. C. Modulation of Lumen Formation by Microgeometrical Bioactive Cues and Migration Mode of Actin Machinery. *Small* **2012**, 10.1002/smll.201202410.
43. Nguyen, M. N.; Lebarbe, T.; Zouani, O. F.; Pichavant, L.; Durrieu, M. C.; Heroguez, V. Impact of RGD Nanopatterns Grafted onto Titanium on Osteoblastic Cell Adhesion. *Biomacromolecules* **2012**, *13*, 896–904.